

ORIGINAL RESEARCH PAPER

Thermal Analysis of Sintered Silver Nanoparticles Film

M. Keikhaie^{1,*}, M.R. Movahhedy¹, J. Akbari^{1,2}, H. Alemohammad³

¹Mechanical Engineering Department, University of Sharif, Tehran, I.R. Iran

²Engineering Design and Manufacture Department, University of Malaya, Kuala Lumpur, Malaysia

³Mechanical and Mechatronics Engineering Department, University of Waterloo, Waterloo, Canada

ARTICLE INFO.

Article history

Received 29 November 2013

Accepted 12 June 2014

Keywords

Heat Flux

Silver Nanoparticles

Thermal Conductivity

Thin Film Propylene Glycol

Abstract

Thin bonded films have many applications in antireflection and reflection coating, insulating and conducting films and semiconductor industries. Thermal conductivity is one of the most important parameter for power packaging since the thermal resistance of the interconnections is directly related to the heat removal capability and thermal management of the power package. The defects in materials play very important role on the effective thermal conductivity. In this paper, finite element method (FEM) was utilized to simulate the effect of pores on the effective thermal conductivity of sintered silver nanoparticles film. The simulation results indicate that the effective thermal conductivity of film is different at different directions and would be enhanced when the pore angle is 90. The simulation results will help us to further understand the heat transfer process across highly porous structures and will provide us a powerful guide to design coating with high thermal insulation or conductor property. Because of there is no similar experimental data for this simulation results, this paper is a comparative work among three different models.

1. Introduction

The thermal conductivity of a thin film is a fundamental material property that is particularly important in high-power/high-frequency micro-electronic devices and micro/nanoscale thermal systems since the ability to dissipate heat is often the limiting factor that determines the device performance. Also, the thermal conductivity of a thin

film may be substantially different from that of the bulk material because of the microstructure [1-3].

This difference is increasingly important, as electronic devices shrink in size and thermal management becomes a limiting factor in performance [4-7].

Rapid progress in the synthesis and processing of materials with structure on nanometer length scales has created a demand for greater scientific understanding of thermal transport in nanoscale devices, individual nanostructures, and nano structured materials.

*Corresponding author

Email address: mahdi.keikhaie@yahoo.com

Nomenclature

A	area of nonlinear thermal gradient region around the defect (m ²)	Q_{sum}	total heat flux (W/m ²)
h	height of element (m)	R	gas constant (J/mol. ⁰ K)
K	thermal conductivity (W/m ⁰ K)	T	absolute temperature (⁰ K)
K_0	thermal conductivity of the non-defective bulk material	W	width of model (m)
K_{eff}	effective thermal conductivity (W/m ⁰ K)	θ	geometric variable
l	length of model (m)	ρ	Porosity
n_0	normal direction of the substrate surface	ΔT	temperature difference (⁰ K)
q	total heat flux per unit thickness (W/m)	∇T	temperature gradient (⁰ K/m)

The experimental difficulties begin with the severely limited capabilities for measuring thermal transport in nanoscale systems. Thus, this paper presents a Finite Element Analysis(FEA) of a nanoscale porous thin film to study influence of pores on heat flux and consequently

thermal conductivity of it, perpendicular to the film surface. We also calculate an independent variable only affected by thermal nonlinear area around pores. Thermal conductivity is the property of a material that indicates its ability to conduct heat. It appears primarily in Fourier's law for heat conduction; as follow

$$\vec{q} = -K\nabla T \quad (1)$$

$$\nabla T = \hat{n}_0 \frac{\Delta T}{dW} \quad (2)$$

where q is the heat flux density (the heat flux density is the amount of energy that flows through a unit area per unit time), K is the thermal conductivity which indicates the material's ability to conduct heat, ∇T is the temperature gradient, and n_0 is parallel to the heat flux direction. ΔT is the temperature difference and dW is the thickness of conducting surface separating the two temperatures.

The thermal conductivity, K , of a material generally varies with temperature; the variation can be small over a significant range of temperatures for some common materials. In this case, assumed K is constant during the simulations.

Wei et al. [8], determined formulation for effects of a defect on effective thermal conductivity of a plate, as follow

$$Q_{sum} = K_{eff} \Delta T.l \quad (3)$$

here Q_{sum} is total heat flux through the plate, K_{eff} is effective thermal conductivity and l is length of plate. If the material of plate is isotropic and plate without defects inside [8],

$$Q_{sum} = \int_s K_0 \cdot (\delta \nabla T)^T \nabla T dS = \int_s K_0 \cdot \frac{\Delta T}{dh} dS = \quad (4)$$

$$K_0 \cdot \frac{\Delta T}{h} \cdot hl = K_0 \cdot \Delta T.l$$

Because of the localized effects caused by defect, a nonlinear thermal gradient area will occur around the defect. Since the thermal conductivity of air (surrounded in defect) is very small as compared to that of the bulk material, zero conductivity is assumed within defect areas. The total thermal flux is rewritten as

$$Q_{sum} = \int_s K_0 \cdot (\delta \nabla T)^T \nabla T dS = \int_B K_0 \cdot \frac{\Delta T}{h} dB + \int_A K_0 \cdot (\delta \nabla T)^T \nabla T dA = K_0 \left\{ \frac{\Delta T}{h} [(1-\rho).hl - A] + \int_A (\delta \nabla T)^T \nabla T dA \right\} \quad (5)$$

where A is area of nonlinear thermal gradient region around the defect. According to Eqs. (3) and (5), K_{eff} can be expressed as [8],

$$K_{eff} = K_0 \left[1 - \rho - \frac{A}{hl} + \frac{\int_A (\delta \nabla T)^T \nabla T dA}{\Delta T.l} \right] \quad (6)$$

By simplifying [8],

$$K_{eff} = K_0 \left(1 - \rho - \frac{C_K}{hl} \right) \quad (7)$$

where K_0 is intrinsic thermal conductivity of the non-defective bulk material, C_K is an independent variable only affected by thermal nonlinear area around the defect and ρ is porosity.

3. Finite Element Results

3.1. Geometrical features

Metallic nanoparticle inks are used in making of thin films in printed electronics. These inks typically consist of silver or gold nanoparticles (nominal particle diameters 2–50 nm). After printing a film, its structure can be obtained by sintering, i.e. by partially melting and fusing the adjacent nanoparticles together. Due to the nanoscale size of the particles, the typical sintering temperatures are only a fraction of the macroscopic melting point of the corresponding materials. Keikhaie et al [9], for a silver nanoparticles (particle diameter 40 nm) layer that arranged tidily and also considered on a rigid substrate (Figure 1), have been calculated sintered configuration of layer for 1 hour annealing time and 150 °C isothermally temperature (Figure 2). In this paper to investigate effects of one pore and all pores on heat flux, used one cell that can see in Figure 2, and all sintered layer, respectively.

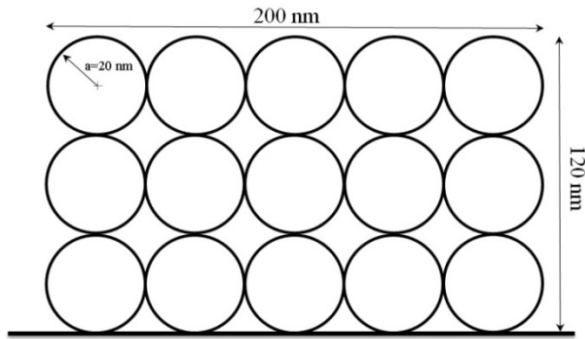


Fig.1. Schematic representation of initial film configuration before sintering process.

3.2. Effects of a pore on the effective thermal conductivity

In this work, to investigate effects of a pore on effective thermal conductivity have been used one cell (Figure 3) with three different orientations ($\theta = 0, 45,$

90 degree).

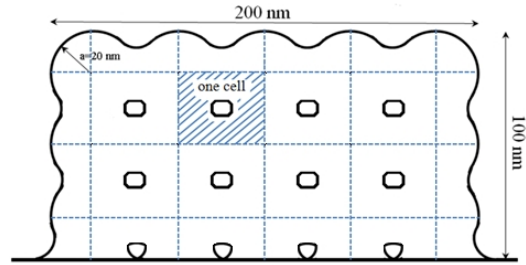


Fig.2. Final film configuration after isothermal sintering at 150 °C and 1 hour.

Top and the bottom of cell are assigned constant temperature of $T + \Delta T$ and T , such that a temperature difference of ΔT is set up across the cell. The other two sides are kept adiabatic. Finite element simulation has been used to measure heat flux crosses from measure line in every model that shown in Figure 4 To simulate the heat flux of sintered nanoscale silver layer, assumed element is perfect and bulk properties of silver are used and they are listed in Table 1 Results of heat flux versus length of three models that crossed from measure line have been plotted in Figure 5 Results show that average of heat flux in model-c is more than model-b and heat flux of model-b is more than model-a ($Q_{sum-c} > Q_{sum-b} > Q_{sum-a}$). It can also be seen that the heat flux in the pore has lowest heat flux (considered that air has 0 thermal conductivity).

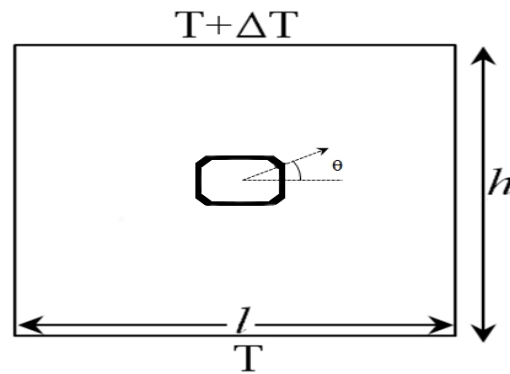


Fig.3. Element plate with pore inside subject to a temperature difference load.

Heat flux vectors of three models also are plotted in Figure 6. As results graphically have been shown in Figure7, in all models the maximum heat flux accumulation occurs in a point that the direction of heat flux is parallel to the contact surface of the hole (2nd point), and the minimum value occurs in a point that the direction of heat flux is perpendicular to the

surface of the hole (3rd point).

Table 1
Properties of silver film

No	Property	Sintered state	Bulk state
1	conductivity ($\frac{W}{m^{\circ}K}$)	240 [10]	430 [11]
2	CTE ($\frac{1}{^{\circ}K}$) $\times 10^{-6}$	19 [10]	19.5 [11]
3	Specific heat ($\frac{J}{Kg^{\circ}K}$)	230 [11]	234 [10]

This is because the holes act like obstacles against the heat flux, so these voids compressed heat flux in sides and distracted from holes' back and consequently the flux increases within the sides of the holes and decreases within them back (Figure 6). Equation 3 dictates that due to the larger contact surface in Figure 6 (c), the heat flux intensity is less than that in Figure 6 (a) and 6 (b), as can be seen..

As said before, C_K is an independent variable only affected by thermal nonlinear area around the pores. Certainly, C_K should be proved to have no relationship with thermal gradient and element size. To determine C_K for different θ and ΔT , has been used Equation 7. The area of the pore and the cell are constant, K_0 for bulk silver is 430 W/m²K and K_{eff} has been calculated by finite element simulation for each models. C_K values are tabulated in Table 2. As seen in Table 2, in different ΔT , C_K didn't change but in different θ , C_K changed. As can be seen, C_K is only affected by thermal nonlinear area around the pore (Figure 6 show different pattern of heat flux vectors around the different pore orientation).

3.3. Thermal conductivity and influence of pores distribution on the heat flux

In previous section, effect of one pore explored. Now, it is time to explore effect of all pores on film's heat flux. To determine the heat flux behavior of a whole film, FEM was also employed to simulate the film with different geometrical arrangements and

orientations of pores. As former modeling for one cell, for whole film was also considered top and the bottom of film have constant temperature of $T + \Delta T$ and T and the left and right boundaries are kept insulated (Figure 8). Figure 9, shows the heat flux distribution of Y direction of film with different arrangements and orientations of pores.

To compare the heat flux in different cases, a measure line in the same position of all models has been drawn (Figure 9). Table 3 shows average heat flux in all models.

It may be concluded from this discussion that the holes geometry with the 90 degree angle transmits the maximum heat flux. However, it can be observed in Figure 9, that the arrangement of holes influences on the heat flux, too. The arrangement in Figure 9 (a) is a normal one and heat flux can pass through all points properly, whereas the arrangement in Figure 9 (b), causes the heat flux to become zigzags and thus cannot pass through all points properly (i.e. because there is less obstacles in front of heat flux in Figure 9 (a) compare to Figure 9 (b)). Therefore the combination of a geometry with an angle of 90 degree and a normal arrangement (figure 12 (e)), transmits the maximum heat flux (see Table 3).

4. Conclusion

In this paper, the influence of different arrangements and orientations of pores on the heat flux and effective thermal conductivity of a sintered silver thin film is investigated. The important results can be summarized as follows:

- (1) C_K is an independent variation of thermal nonlinear area around the pore, which is only affected by the pore's orientation.
- (2) When the pores area is fixed, different orientation of pores will have different thermal conductivity effect.
- (3) Porous film with normal arrangement and 90-degree orientation has the most heat flux transition.

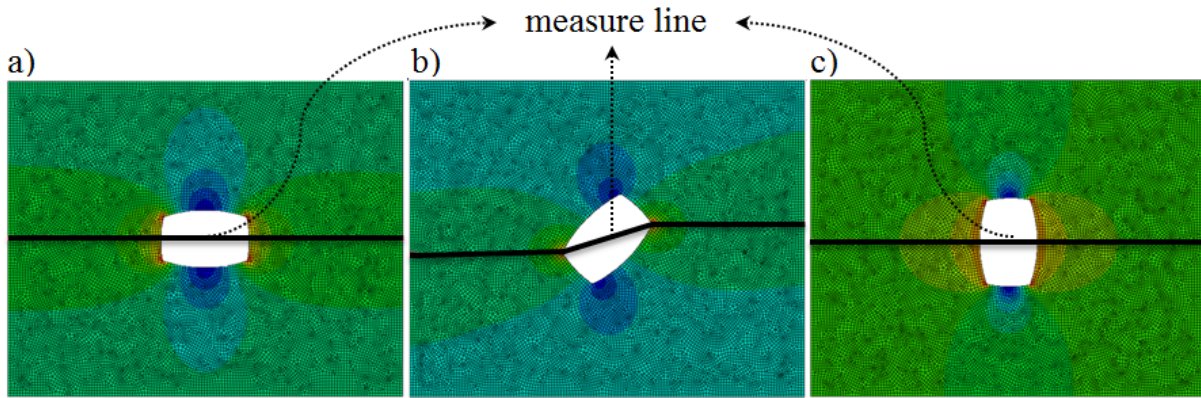


Fig. 4. FEM results of heat flux for different pore's orientations.

Table 2

C_K values with different pore's orientations and ΔT

Model	ΔT ($^{\circ}K$)	S_{model} (nm^2)	S_{pore} (nm^2)	ρ (S_{pore}/S_{model})	K_{eff}/K_0	C_K
A	1	1280	45	0.03515625	0.906554773	74.60989059
a	10	1280	45	0.03515625	0.906554773	74.60989059
a	100	1280	45	0.03515625	0.906554773	74.60989059
b	1	1280	45	0.03515625	0.924403317	51.76375387
b	10	1280	45	0.03515625	0.924403317	51.76375387
b	100	1280	45	0.03515625	0.924403317	51.76375387
c	1	1280	45	0.03515625	0.940039	31.75007978
c	10	1280	45	0.03515625	0.940039	31.75007978
c	100	1280	45	0.03515625	0.940039	31.75007978

Table 3

Average heat flux for different models

Model	Average heat flux
2. a	282.6215483
2. b	251.9624689
2. c	285.5741012
2. d	254.1324651
2. e	288.9946414
2. f	257.9950207

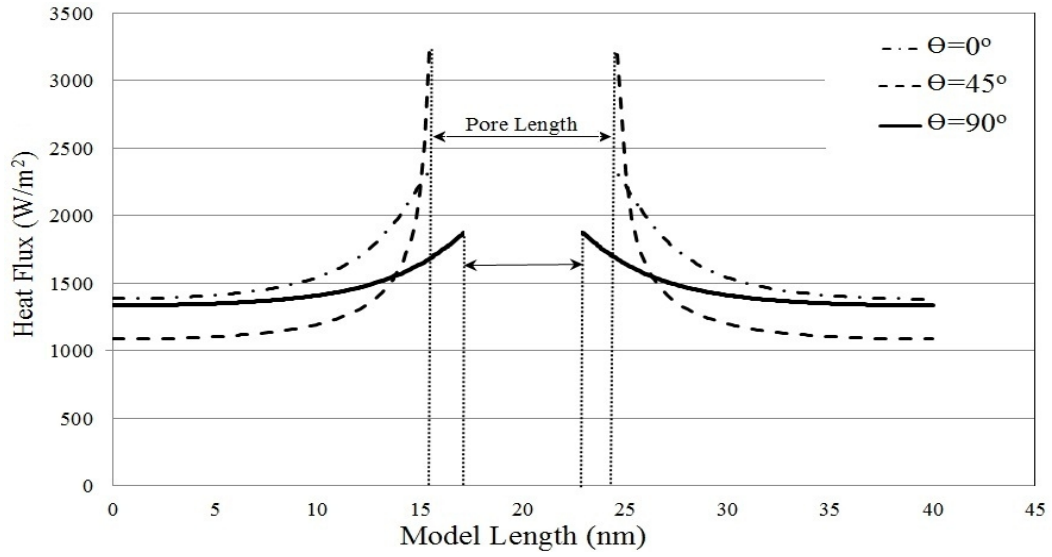


Fig. 5. Heat flux values cross measure line for different pore's orientations.

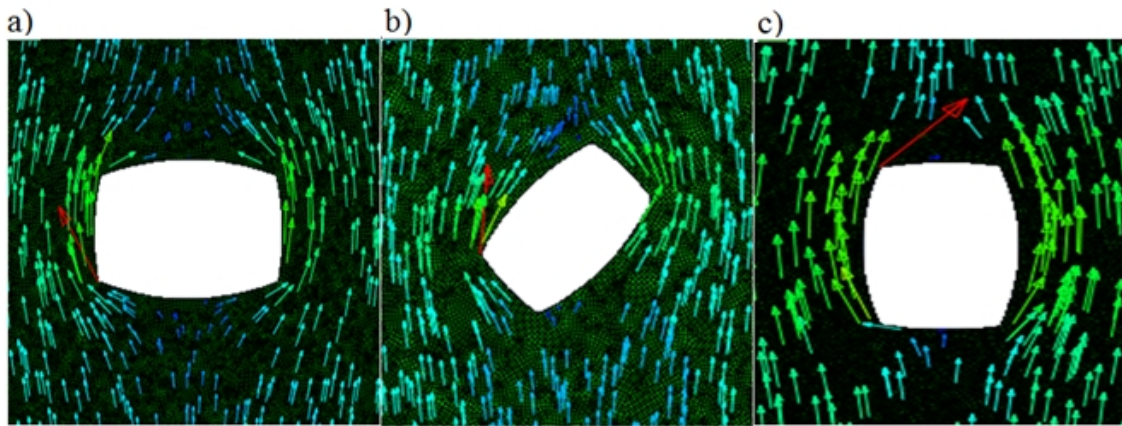


Fig. 6. Heat flux vectors around pore in different orientations.

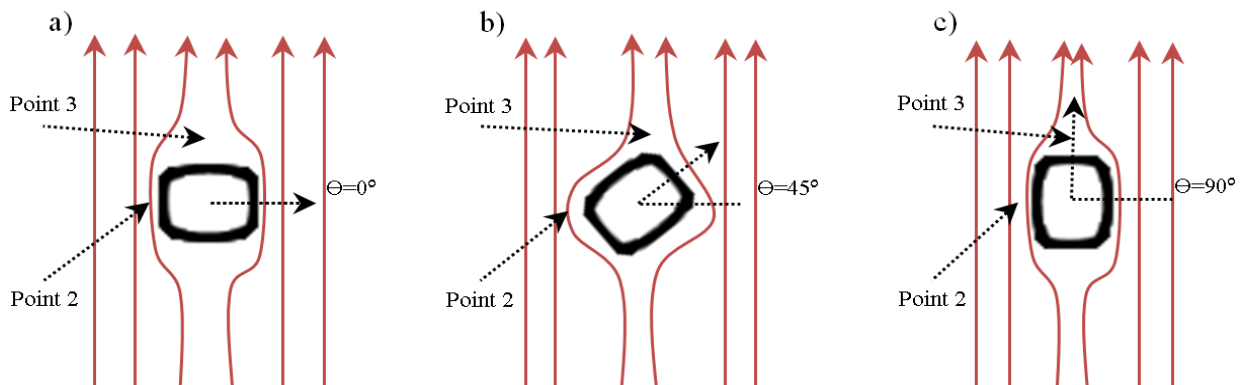


Figure 7. Heat flux flow around pore in different orientations.

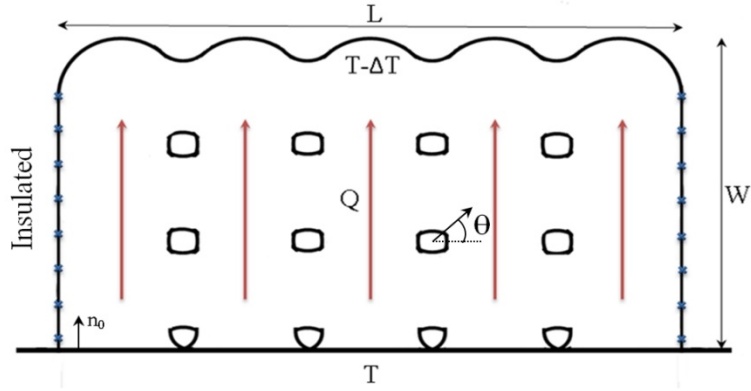


Fig. 8. Model is used to simulate heat flux in Y direction.

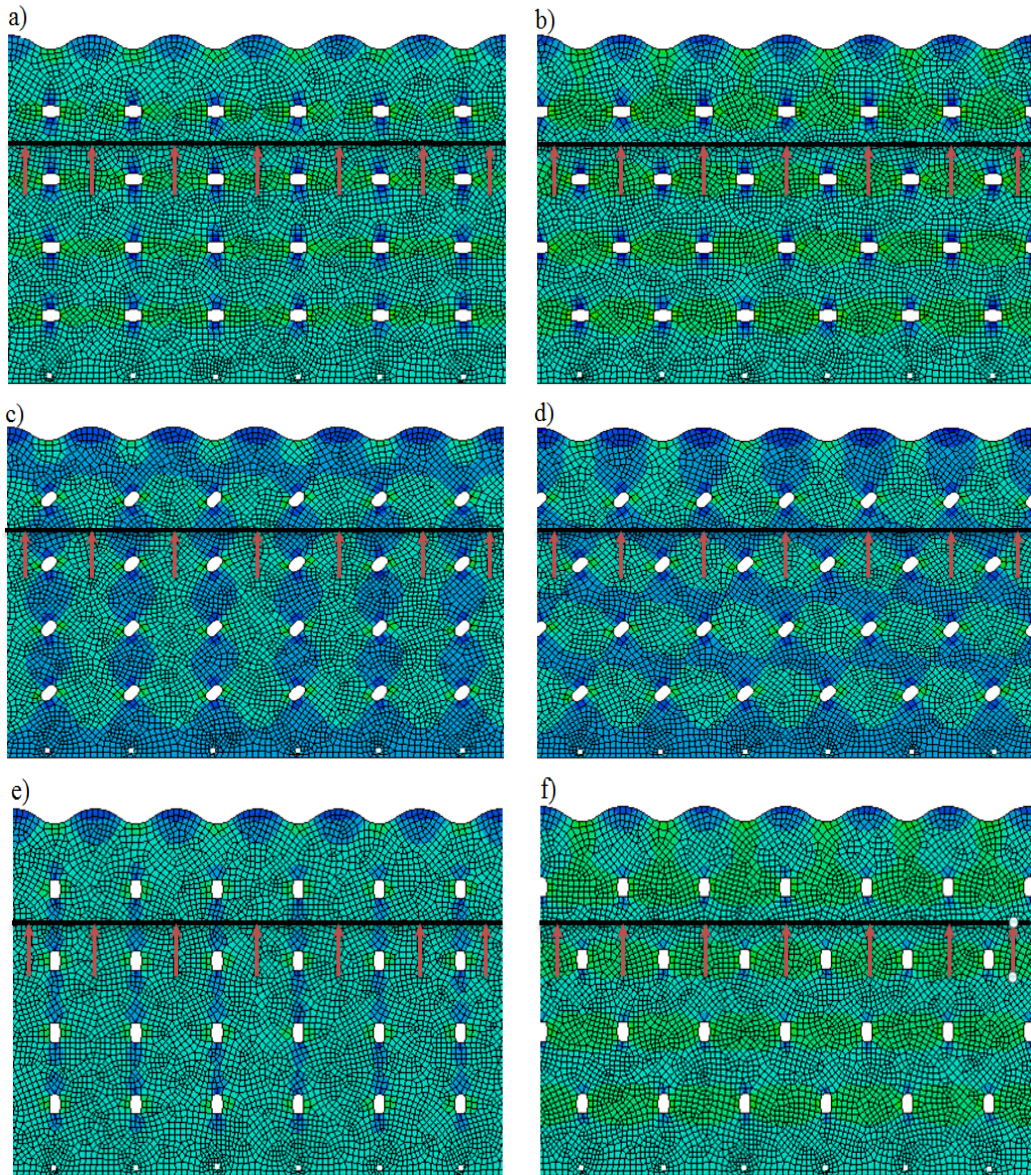


Fig. 9. Simulation results of heat flux for a) angle-0 and straight arrangement b) angle-0 and zigzag arrangement c) angle-45 and straight arrangement d) angle-45 and zigzag arrangement e) angle-90 and straight arrangement f) angle-90 and zigzag arrangement.

References

- [1] D.G. Cahill, H.E. Fischer, T. Klitsner, E.T. Swartz, R.O. Pohl, Thermal conductivity of thin films: Measurement and understanding, *J. Vac. Sci. Technol. A, Vac. Surf. Films* 7 (1989) 1259–1266.
- [2] S.M. Lee, D.G. Cahill, Heat transport in thin dielectric films, *J. Appl. Phys* 81 (1997) 2590–2595.
- [3] K.E. Goodson, M.I. Flik, L.T. Su, D.A. Antoniadis, Annealing temperature dependence of the thermal conductivity of LPCVD silicon dioxide layers, *IEEE Electron Device Lett* 14 (1993) 490–492.
- [4] I. Ahmad, V. Kasisomayajula, D.Y. Song, L. Tian, J.M. Berg, M. Holtz, Self-heating in a GaN based heterostructure field effect transistor: Ultraviolet and visible Raman measurements and simulations, *J. Appl. Phys.* 11 (2006) 113718-1–113718-7.
- [5] D.G. Cahill, W.K. Ford, K.E. Goodson, G.D. Mahan, A. Majumdar, H.J. Maris, R. Merlin, S.R. Phillpot, Nanoscale thermal transport, *J. Appl. Phys.*, 93, 2 (2003) 793–81.
- [6] D.L. DeVoe, Thermal issues in MEMS and microscale systems, *IEEE Trans. Compon. Packag. Technol* 25 (2003) 576–583.
- [7] X. Liu, M.H. Hu, C.G. Caneau, R. Bhat, C. Zah, Thermal management strategies for high power semiconductor pump lasers, *IEEE Trans. Compon. Packag. Technol* 29 (2006) 493–500.
- [8] Sh. Wei, W. Fu-chi, F. Qun-Bo, M. Zhuang, Effects of defects on the effective thermal conductivity of thermal barrier coatings, *Applied Mathematical Modelling* 36 (2012) 1995–2002.
- [9] M. Keikhaie, J. Akbari, M.R. Movahhedi, H.R. Alemohammad, Sintering Characterizations of Ag-nano Film on Silicon Substrate, *Advanced Materials Research* 829 (2014) 342-346.
- [10] Y. Mei, G. Chen, G. Lu, X. Chen, Effect of joint sizes of low-temperature sintered nano-silver on thermal residual curvature of sandwiched assembly, *International Journal of Adhesion & Adhesives* 35 (2012) 88–93.
- [11] D.R. Smith, F.R. Fickett, Low-Temperature Properties of Silver, *Journal of Research of the National Institute of Standards and Technology* 2 (1995).